Amide Modes of the α-Helix: Raman Spectroscopy of Filamentous Virus *fd* Containing Peptide ^{13}C and ^{2}H Labels in Coat Protein Subunits†

Stacy A. Overman and George J. Thomas, Jr.*

Division of Cell Biology and Biophysics, School of Biological Sciences, University of Missouri−Kansas City, Kansas City, Missouri 64110

Received September 22, 1997; Revised Manuscript Received March 2, 1998

ABSTRACT: The filamentous virus *fd* consists of a single-stranded DNA genome sheathed by 2700 copies of a 50-residue α-helical subunit (protein pVIII) and serves as a model assembly of α-helices. To advance vibrational assignments for the α-helix, we have investigated Raman spectra of *fd* virions containing ^{13}C and ^{2}H (deuterium) labels at various main-chain sites of the pVIII subunits. ^{13}C was introduced at specific peptide carbonyls, while deuterium was introduced at selected α-carbon (C_α) and amide nitrogen positions. Interpretation of the Raman spectra reveals a previously unrecognized α-helix band in the spectral interval 730−745 cm^{-1}, tentatively assigned to a carbonyl in-plane bending mode (amide IV). Experimental evidence has also been obtained for a distinctive α-helix marker near 1345 cm^{-1}, assigned to a coupled C_α−H bending and C_α−C stretching mode. The *fd* virions containing ^{13}C-labeled carbonyls exhibit unexpectedly complex amide I profiles, consisting of multiple band components. Amide I splitting resulting from ^{13}C substitution of carbonyls is attributed to decoupling of transition-dipole interactions normally occurring in the extended pVIII helix. The present study identifies novel conformation-dependent Raman bands in a native α-helix assembly, confirms amide I and amide III assignments proposed previously for filamentous viruses, and facilitates new Raman assignments for the packaged ssDNA. The α-helix markers identified here should also be useful in conformation analyses of other proteins by Raman spectroscopy.

Ff is the class prototype of long (≈880 nm) and thin (≈6 nm) bacterial viruses infecting F^+ strains of *Escherichia coli*. The *Ff* class includes phages *fd*, *f1*, and *M13*, of which *fd* has been investigated most extensively with respect to virion architecture. In the mature *fd* particle, which is composed mainly (87 wt %) of coat protein, a covalently closed and single-stranded (ss)[1] DNA genome of 6407 nucleotides is packaged within a sheath of 2700 copies of the 50-residue coat subunit, pVIII (sequence: ^{1}AEGDDPAKAA ^{11}FDSLQASATE ^{21}YIGYAWAMVV ^{31}VIVGATIGIK ^{41}LFKKFTSKAS). Further details of the assembly pathway have been reviewed by Webster (*1*). Diffraction and spectroscopic studies (*2*−*17*) of *fd* reveal a uniformly α-helical pVIII subunit that is tilted on average from the virion axis by approximately 16°. Subunits are layered about the axis with 5-fold rotational symmetry and an approximate 2-fold screw axis. Results from randomized mutagenesis experiments support close packing of pVIII α-helices in the native virion (*18*). Accordingly, *fd* is an ideal model for an assembly of α-helical proteins. Here, we investigate isotope-edited variants of this model α-helix assembly by Raman spectroscopy and consider the implications of the results for Raman studies of other α-helical proteins.

Many details of protein structure, including main-chain conformation, can be probed effectively by Raman spectroscopy. Vibrational modes characteristic of the trans peptide group—referred to as amide modes (*19*)—generate intense Raman spectral bands that are sensitive to the protein secondary structure and serve as empirical markers of α-helix, *β*-strand, and irregular conformations (*20*). A comprehensive review of empirical spectra−structure correlations has been given recently (*21*). Frequently utilized are the amide I band (1645−1680 cm^{-1} interval), which originates mainly from peptide C═O stretching, and the amide III band (1230−1310 cm^{-1} interval), which involves a combination of peptide N−H bending and C−N stretching motions.

To complement empirical correlations, the amide I and amide III modes have been investigated in great detail, both theoretically and experimentally, in peptide model compounds and peptide oligomers (*19*−*22*). Among the practical techniques utilized to enhance the interpretive value of peptide Raman spectra is site-specific isotopic substitution. Indeed, isotope substitution is often the method of choice for reaching definitive vibrational assignments. Studies of ^{2}H (D), ^{13}C, ^{15}N, and ^{18}O isotopomers of the peptide group have been reported (*23*−*26*). Surprisingly, however, no detailed Raman (or infrared) studies have been reported on native proteins incorporating stable isotopes, other than deuterium, in main-chain moieties. Consequently, the in-

† Paper LXII in the series Structural Studies of Viruses by Raman Spectroscopy. Supported by NIH Grant GM50776.

* To whom correspondence may be addressed.

[1] Abbreviations: NMA, *N*-methylacetamide; D or ^{2}H, deuterium; *fd*(*n*X^{13}C), *fd* virion containing ^{13}C-labeled peptide carbonyls at the *n* residues of amino acid X in the pVIII subunit; *fd*(D_2O), *fd* virion exchanged in D_2O by incubation for 40 h at 50 °C; *fd*($10A_{d1}$), *fd* virion containing $C_\alpha DC_\beta H_3$ at the 10 alanine residues per pVIII subunit; *fd*($10A_{d3}$), *fd* virion containing $C_\alpha HC_\beta D_3$ at the 10 alanine residues per pVIII subunit; *fd*($10A_{dd}$), *fd* virion containing $C_\alpha DC_\beta D_3$ at the 10 alanine residues per pVIII subunit; ssDNA, single-stranded DNA; TDC, transition-dipole-coupling; UVRR, ultraviolet resonance Raman.

S0006-2960(97)02339-8 CCC: $15.00 © 1998 American Chemical Society
Published on Web 04/02/1998

ternal coordinates contributing to Raman amide bands of native proteins are not as well delineated as those of simple peptide analogues. A related issue of current interest is the assignment of Raman bands in the 1300−1350 cm^{-1} spectral interval of the model peptide *N*-methylacetamide (NMA). The spectral range in question encompasses both the amide III vibration and the C−H bending vibrations and has been the subject of conflicting interpretations (*27, 28*).

To advance understanding of amide modes and related main-chain vibrational modes of native protein α-helices, ^{13}C and deuterium labels have been introduced into coat protein peptide groups of the mature *fd* virion. Raman spectra of the labeled viruses have been carefully compared with those of unlabeled *fd*. The *fd* isotopomers were prepared by growth of phage in minimal media supplemented with appropriately labeled amino acids. ^{13}C was introduced into the main-chain carbonyl groups of as many as 37 of the 50 residues per subunit. Deuterium was substituted for protium at the α-carbon (C_α) site of each of the 10 alanine residues per subunit. Additionally, virtually all 49 of the peptide NH groups per subunit were exchanged by incubation of *fd* in D_2O solution. Raman spectra of the *fd* isotopomers are interpreted to clarify both amide band assignments and related main-chain vibrational assignments of the native α-helix assembly. The results provide new insights into conformation-sensitive features of the Raman spectrum of the α-helix. Improved understanding of the vibrational fingerprint of *fd* α-helices is also expected to shed further light on assignments for NMA and other model peptides. Finally, we note that the present comparative analysis of labeled and unlabeled *fd* provides new spectroscopic and structural information relating to the packaged ssDNA genome.

MATERIALS AND METHODS

1. Preparation of Virus. Stocks of wild-type *fd* virus were obtained from Dr. Loren A. Day, Public Health Research Institute, New York, and grown on *Escherichia coli* strain Hfr3300. Growth media and standard reagents were obtained from Sigma Chemical (St. Louis, MO) and Fisher Scientific (St. Louis, MO). Deuterium- and ^{13}C-labeled amino acids were obtained from Cambridge Isotope Laboratories (Woburn, MA).

Unlabeled virus was grown in MS medium containing 1% glucose and 4 mM $CaCl_2$. Mature viral particles, extruded through the bacterial cell membrane and into the growth medium, were collected by precipitation with poly(ethylene glycol) (2%) and NaCl (0.5 M) followed by low-speed centrifugation. The virus precipitate was resuspended in 10 mM Tris (pH 7.8 ± 0.2), and the resulting suspension was purified in four cycles of pelleting by centrifugation at 330000*g* for 1.5 h and resuspension of the pellet in 10 mM Tris buffer. This procedure accomplishes essentially complete removal of excess NaCl and produces the low-salt form of the virus. (The effect of salt concentration on the Raman spectrum of *fd* has been reported elsewhere (*5*).) Typically, 30−40 mg of purified virus was obtained from a 1-L preparation. Virus concentration was determined by UV spectrophotometry using an extinction coefficient at 270 nm of 3.84 $mL \cdot mg^{-1} \cdot cm^{-1}$ (*29*).

For specific ^{13}C labeling, host and virus were grown in M9 minimal medium containing 10 μg/mL thiamine hydrochloride, 1% glucose, each unlabeled L-amino acid at 0.1 mM, and each labeled L-amino acid at $n \times 0.1$ mM, where *n* is the number of residues of the given amino acid in the pVIII sequence (above). Similar methods have been used previously (*14, 30*). Mature viral particles were isolated as described above and purified on a continuous (1.257 g/mL) KBr gradient in a swinging-bucket rotor at 247000*g* for 48 h at 4 °C. The virus band was collected, diluted 2-fold with 10 mM Tris, and subjected to four cycles of centrifugation and resuspension to remove excess KBr. Typically, 20 mg of purified virus was obtained from a 1-L preparation. The following ^{13}C-carbonyl-labeled *fd* variants were prepared: *fd*(10A^{13}C), labeled at the 10 alanines per subunit; *fd*(4V^{13}C), labeled at the 4 valines; *fd*(4G^{13}C), labeled at the 4 glycines; and *fd*(37^{13}C), labeled at 37 residues (10A + 3F + 4G + 4I + 5K + 4S + 3T + 4V). [Note that because 1 of the ^{13}C labels of *fd*(37^{13}C) is located at the C-terminal serine of pVIII, the subunit contains 36 labeled peptides plus 1 labeled carboxyl group.)]

The *fd* isotopomer containing deuterium at each of the 10 alanine C_α sites, designated *fd*($10A_{d1}$), was prepared by growing *fd* in minimal medium (described above) that contained alanine-d_1. The virus was isolated, purified, and concentrated as described above.

Deuterium labeling of peptide amide groups was accomplished by exchange of *fd* in D_2O. The virus was resuspended in 10 mM Tris−D_2O (pD 8.2), and then subjected to three incubation protocols: (i) 4 °C for 20 h, (ii) 50 °C for 20 h, (iii) 60 °C for 500 h. Samples (i), (ii), and (iii), representing different levels of H/D exchange, were pelleted at 330000*g* for 1.5 h at 4 °C. The resuspension in D_2O and incubation procedure was then repeated for samples (i) and (ii), yielding virions exchanged for 40 h at 4 and 50 °C, respectively. For sample (iii), 2 mM borate−D_2O (pD 9.35) was used in place of 10 mM Tris−D_2O as the final resuspension buffer, and the incubation procedure was not repeated. In the following sections, sample (ii) is referred to as *fd*(D_2O).

2. Isolation of Circular, Single-Stranded fd DNA. The circular ssDNA genome was extracted from unlabeled *fd* by two cycles of treatment with a 10 mM Tris-saturated phenol mixture. The DNA was precipitated from the aqueous phase in 20 h by treatment with 2 volumes of ethanol at −20 °C, partially dried, and resuspended in 3.0 mL of 10 mM Tris, 1 mM EDTA (pH 7.2). The ssDNA product was very pure as indicated by the high UV absorbance ratio, $A_{260}/A_{280} = 1.93$. The protein-free ssDNA was concentrated for Raman spectroscopy using a Centricon concentrator (Amicon, Inc., Beverly, MA).

The purified *fd* ssDNA was characterized by gel electrophoresis (2.5 V/cm, 20 h) in 30 mM NaOH, 1.5% agarose at 22 °C. Covalently closed *M13* ssDNA (7249 bases; Bio-Rad Laboratories, Hercules, CA) was used as a control. The DNA was stained with SYBR green (Molecular Probes, Inc., Eugene, OR) and visualized under a UV lamp. Other details of the electrophoresis experiment were as described by Shin and Day (*31*). Comparison of the gel migration patterns of the two ssDNA circles with one another and with published data (*31*) confirmed that the isolated *fd* ssDNA was predominantly circular (i.e., covalently closed) and consisted of the expected number of nucleotides.

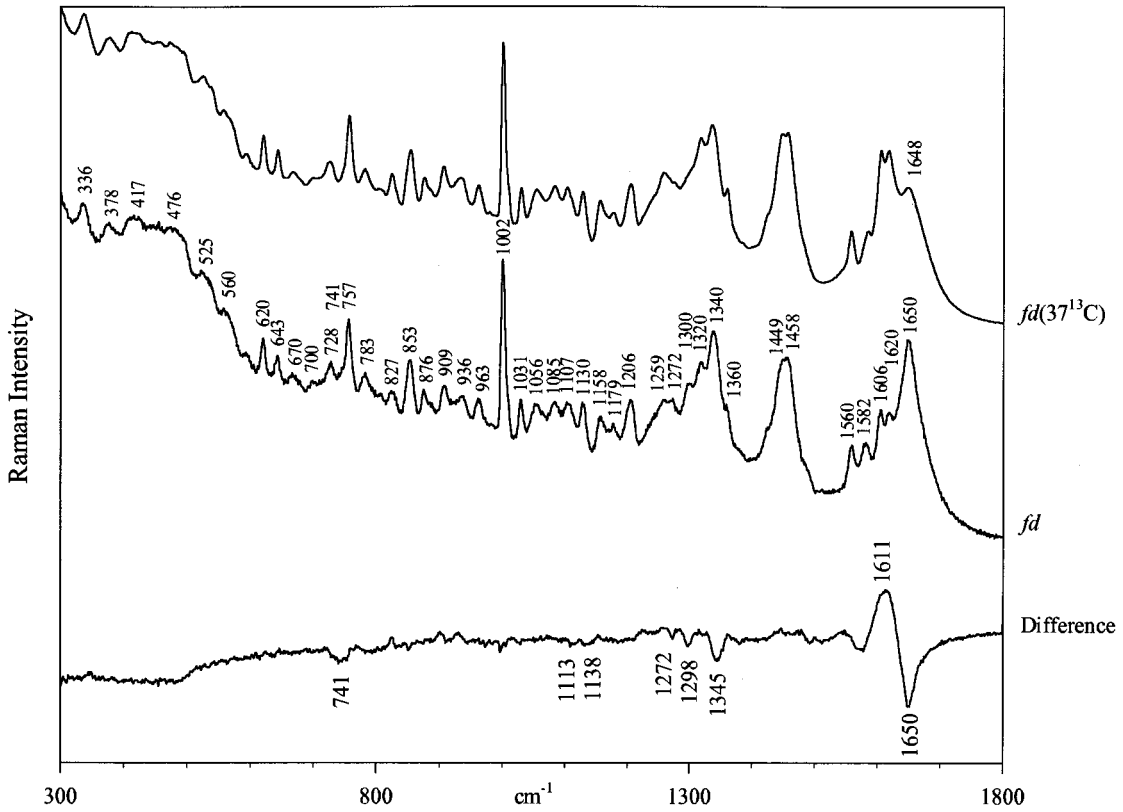

FIGURE 1: Top: Raman spectrum (300−1800 cm^{-1}) of *fd*($37^{13}C$), an *fd* isotopomer containing ^{13}C-carbonyl labeling at 36 peptide sites (10A + 3F + 4G + 4I + 5K + 4S + 3T + 4V) of the 50-residue coat subunit. Middle: Raman spectrum of unlabeled *fd*. Bottom: Difference spectrum computed with *fd*($37^{13}C$) as minuend and unlabeled *fd* as subtrahend and normalized to minimize spectral differences of aromatic marker bands at 620, 643, 757, 1002, and 1206 cm^{-1}, which are insensitive to ^{13}C-carbonyl labeling. Spectra were obtained from 80 mg/mL solutions of virus in 10 mM Tris buffer, pH 7.8.

3. Raman Spectroscopy. Virus solutions were prepared at ≈80 mg/mL, sealed in standard glass capillaries, and thermostated at 12 °C for Raman analysis (*32*). Typically, a 2 μL aliquot was sufficient to fill the portion of the sample cell exposed to laser illumination. Spectra were excited at 514.5 nm with an argon laser (Innova 70, Coherent Inc., Santa Clara, CA) and recorded on a scanning double spectrometer (Ramalog V/VI, Spex Industries, Edison, NJ) with photon-counting detector (Model R928P, Hamamatsu, Middlesex, NJ). Data at 1.0 cm^{-1} intervals were collected with an integration time of 1.5 s and a spectral slit width of 8 cm^{-1}. Samples were scanned repetitively, and individual scans were displayed and examined prior to averaging. The spectrometer was calibrated with indene and carbon tetrachloride. Frequencies cited are accurate to ±1 cm^{-1} for well-resolved peaks and ±2 cm^{-1} for very broad bands or shoulders. Further details of the instrumentation and data collection protocols are given elsewhere (*30*, *33*). Spectra were compared by digital difference methods using SpectraCalc software (Galactic Industries, Salem, NH). Ordinarily, difference spectra were computed prior to correcting the raw data for contributions of solvent and background. This allowed differentiation of subtle changes that might otherwise have been difficult to detect and avoided introduction of artifacts from incomplete solvent or background compensation in spectral components of the subtraction (*30*).

RESULTS

Figure 1 compares the Raman spectrum of *fd*($37^{13}C$) with that of unlabeled *fd*. Frequencies of normal vibrations involving displacement of main-chain carbonyl C atoms are revealed as peaks ($^{13}C{=}O$ isotopomer) or troughs ($^{12}C{=}O$ isotopomer) in the Figure 1 difference spectrum. In computing this difference spectrum, the parent spectra were normalized to compensate prominent Raman markers of aromatic side chains that are invariant to peptide isotope substitution (*14*). Figure 2 compares Raman spectra of several ^{13}C-labeled *fd* isotopomers with one another and with unlabeled *fd*.

Figure 3 compares the Raman spectrum of the deuterium-exchanged virion, *fd*(D_2O), with that of unlabeled *fd*. In the Figure 3 difference spectrum, peaks represent vibrational frequencies of deuterium-exchanged residues, while troughs represent frequencies of the corresponding protium form. Because of the large number of exchangeable sites (amide NH, side-chain OH and NH, and NH and NH_2 groups of packaged DNA), a very rich difference spectrum is generated by D_2O exchange.

Figure 4 compares the 1250−1400 cm^{-1} interval of the Raman spectrum of *fd*($10A_{d1}$) with that of unlabeled *fd*. As evident in the Figure 4 difference spectrum, deuterium labeling of the C_α atom of the 10 alanine residues in pVIII causes a loss of intensity at 1345 cm^{-1} and a corresponding intensity gain at 1296 cm^{-1}. [A similar difference profile occurs between the isotopomers *fd*($10A_{d4}$) and *fd*($10A_{d3}$), which are likewise distinguished only by the hydrogen isotope at alanine C_α sites (*34*).]

Figures 5 and 6 compare Raman spectra of H_2O and D_2O solutions of tryptophan (W), tyrosine (Y), lysine (K), threonine (T), serine (S), and glutamine (Q), which are the

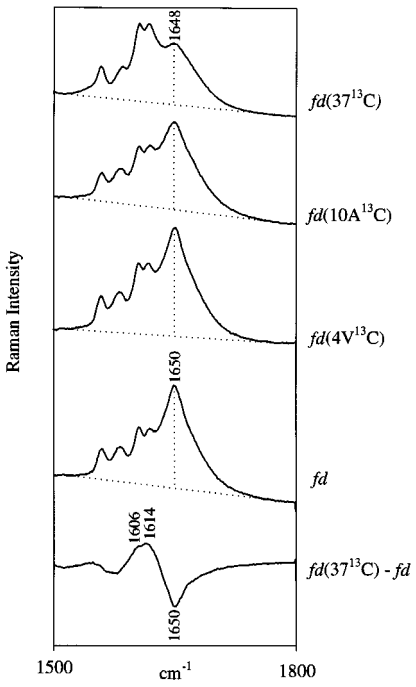

FIGURE 2: Comparison of Raman spectra of ^{13}C-labeled and unlabeled *fd* in the region 1500−1800 cm^{-1}. From top to bottom: *fd*(37^{13}C), *fd*(10A^{13}C), *fd*(4V^{13}C), unlabeled *fd*, and the *fd*(37^{13}C) − *fd* difference spectrum. These data demonstrate the progressively increasing perturbations to bands of the amide I region (1600−1700 cm^{-1}) resulting from the greater number and dispersion of ^{13}C substitution of peptide carbonyls, as discussed in the text.

pVIII amino acids with exchangeable side chains. Figure 7 compares Raman spectra of H_2O and D_2O solutions of the ssDNA circle isolated from *fd*. Raman band shifts accompanying base amino and imino exchanges are indicated in the Figure 7 difference spectrum. Exchange-sensitive Raman bands of Figures 5−7 are expected to contribute to the deuterium-exchange profiles of *fd* that are represented in Figures 3 and 8. Figure 8 illustrates progressive deuterium exchange of pVIII peptide sites. The region 3000−3600 cm^{-1} of Figure 8 also contains bands due to exchange-resistant peptide NH groups.

The foregoing results (Figures 1-8) are discussed and interpreted in the following sections.

DISCUSSION

1. Overview of Isotope Shifts. Incorporation of ^{13}C into 37 of 50 main-chain carbonyls of the *fd* subunit produces intensity decreases at 741, 1113, 1138, 1272, 1298, 1345, and 1650 cm^{-1}, as indicated by the labeled troughs in the difference spectrum [*fd*(37^{13}C) − *fd*] of Figure 1. Additionally, the amide I band at 1650 cm^{-1} is significantly broadened (Figure 2). Similar spectral perturbations result from more limited ^{13}C incorporation (Figure 2).

Deuterium exchange of *fd* eliminates or diminishes Raman bands at 675, 728, 760, 784, 807, 878, 908, 1055, 1085, 1107, 1130, 1251, 1278, 1299, 1343, 1367, 1428, 1492, 1566, 1582, 1621, and 1657 cm^{-1}. Because D_2O exchange of *fd* can deuterate the peptide main-chain, as well as side-chain (NH and OH) and DNA (NH and NH_2) sites, interpretation of the difference spectrum of Figure 3 is not straightforward. However, data of Figures 5−7 and previously published spectra (*14*) permit assignment of troughs at 1278, 1299, 1343, and 1657 cm^{-1} (Figure 3) to pVIII peptide groups and all other troughs to pVIII side chains or packaged DNA.

The present analysis identifies 7 amide-related bands of the pVIII α-helix, 18 bands due to specific pVIII side chains, and 5 bands due to packaged ssDNA in the Raman spectrum of the native virion.

2. Raman Bands Associated with Main-Chain Vibrations of the Coat Protein. The *fd* Raman bands at 741, 1107, 1130, 1272, 1300, 1340, and 1650 cm^{-1} (Figure 1) suffer intensity loss with either ^{13}C or D labeling of pVIII peptide groups. Therefore, they are assigned to modes involving either C═O, C_α−C, C−N, or N−H internal coordinates.

(a) Amide I. The *fd* amide I vibration, which involves mainly C═O stretching and, to lesser degrees, C−N stretching, C_α−C−N bending, and N−H in-plane bending of α-helical peptide groups (*22*), has been assigned unambiguously to the intense band at 1650 cm^{-1} (*3*). In deuterated *fd*, the counterpart to amide I, viz., amide I′, is revealed as an intense band at 1642 cm^{-1}. In the corresponding difference spectrum, the amide I′ peak appears at 1637 cm^{-1} (Figure 3). Because peptide deuteration is not complete (∼85%, see below), the difference spectrum is considered to provide the more reliable estimate of the amide I′ band position, i.e., 1637 cm^{-1}. A similar determination of amide I′ for the pVIII α-helix has been made previously (*35*).

^{13}C labeling of most (37 of 50) main-chain carbonyls of the *fd* subunit generates a complex band profile between 1600 and 1650 cm^{-1} as seen in Figure 1. The corresponding difference spectrum indicates that ^{13}C labeling shifts amide I from 1650 cm^{-1} to approximately 1611 cm^{-1} (here designated amide I^{13C}). The expanded difference profile of Figure 2 further reveals at least two components to amide I^{13C}: at 1606 and 1614 cm^{-1}. The remaining 13 unlabeled peptide groups of *fd*(37^{13}C) contribute a "residual" amide I band at 1648 cm^{-1}. Figure 2 shows that while the frequency of the residual amide I band of *fd*(37^{13}C) is nearly unchanged from that of *fd* (1648 vs 1650 cm^{-1}), the apparent band half-width ($\Delta\sigma_{1/2}$) is considerably increased (30 vs 24 cm^{-1}, or $\Delta\Delta\sigma_{1/2} \approx 6$ cm^{-1}). Two explanations can be offered for the apparent increase in residual amide I bandwidth with ^{13}C labeling. On one hand, carbonyl groups from subunit side chains and DNA bases are expected to contribute Raman intensity in the spectral region 1660−1700 cm^{-1}. This would provide a larger relative intensity contribution to the wing of the 1648 cm^{-1} marker of *fd*(37^{13}C) than to that of the 1650 cm^{-1} marker of *fd*, giving the appearance of a broader residual amide I band in the former spectrum. Alternatively, the greater breadth of the residual amide I band of *fd*(37^{13}C) could result from the elimination of what is known as transition-dipole-coupling (TDC) (*36*−*38*). TDC is a resonance interaction that can occur between dipole moments of neighboring oscillators in different eigenstates. Calculation of TDC effects on Raman amide I bands of α-helices of differing length predicts greater band dispersion for shorter helical segments (<10 residues) than for longer segments (30−65 residues) (*39*). The argument can be made that intermittent ^{13}C-peptide labeling of the pVIII helix, as occurs here (37 of 50 residues), uncouples the otherwise coupled ^{12}C═O oscillators, diminishes putative TDC effects, and leads to broadening of the amide I envelope. Uncoupling would occur because amide I and amide I^{13C} modes are not

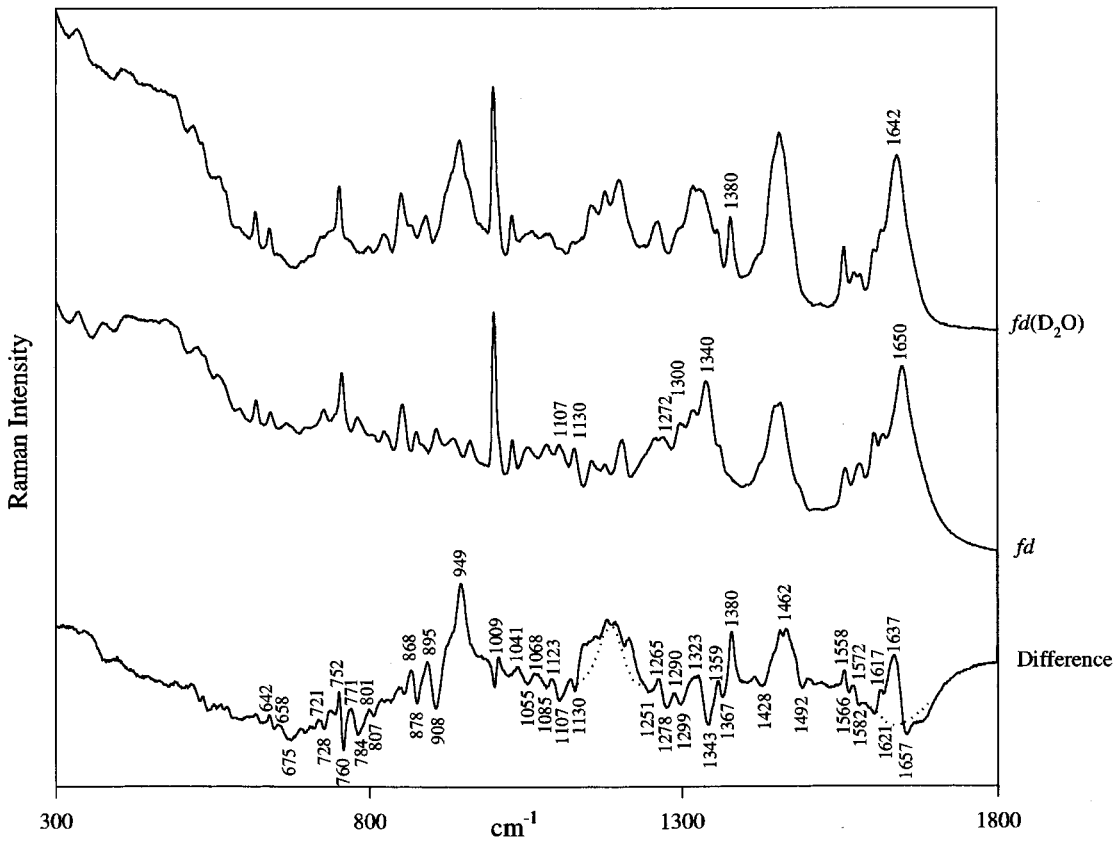

FIGURE 3: Top: Raman spectrum (300−1800 cm^{-1}) of *fd*(D_2O). Middle: Raman spectrum of unlabeled *fd*. Bottom: Difference spectrum computed with *fd*(D_2O) as minuend and unlabeled *fd* as subtrahend and normalized to compensate intensities of phenylalanine bands (620, 827, and 1002 cm^{-1}) that are insensitive to deuterium exchange. Uncompensated contributions of H_2O and D_2O to the difference spectrum are indicated by the dotted contours centered near 1633 and 1205 cm^{-1}, respectively. *fd*(D_2O) was prepared by two cycles of resuspension of *fd* from 10 mM Tris−D_2O (pD 8.2) and incubation at 50 °C for 20 h (40 h total).

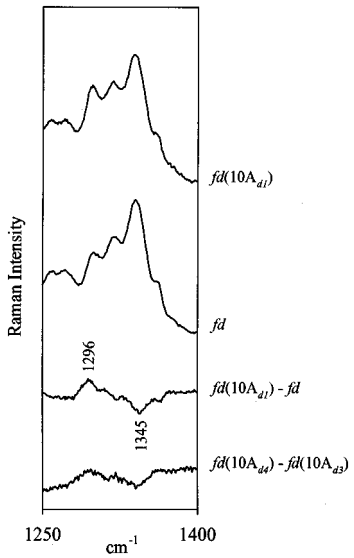

FIGURE 4: From top to bottom: Raman spectrum (1250−1400 cm^{-1}) of *fd*($10A_{d1}$), an *fd* isotopomer containing deuterium labeling only at the C_α group of each of the 10 alanine residues of pVIII; Raman spectrum of unlabeled *fd*; Raman difference spectrum [*fd*($10A_{d1}$) − *fd*]; Raman difference spectrum [*fd*($10A_{d4}$) − *fd*($10A_{d3}$)]. The trough at 1345 cm^{-1} in each difference spectrum is assigned to the peptide backbone mode involving C_α−H bending and C−C_α stretching. (See text.)

sufficiently close for strong TDC resonance interaction. Thus, TDC could explain why the Raman amide I band (1650 cm^{-1}) of unlabeled *fd* is relatively narrow, whereas the amide I^{13C} (1611 cm^{-1}) and amide I (1648 cm^{-1}) bands of *fd*($37^{13}C$) are relatively broad.

Curve-fitting and deconvolution operations (*40*) performed on the amide band profiles of *fd* and *fd*($37^{13}C$) and examination of Raman spectra of amino acid model compounds (unpublished results of S. A. Overman and G. J. Thomas, Jr.) indicate that carbonyl bands from subunit side chains (3D + 2E + 1Q) and DNA bases are insufficient to account for the broadening of amide I seen in Figure 2. Accordingly, our tentative conclusion is that the observed amide I broadening is due mainly to elimination of TDC effects. Another line of experimental evidence in support of TDC comes from the amide I band perturbations produced by more limited ^{13}C labeling of the pVIII main chain. For example, Figure 2 illustrates that the amide I broadening effect observed for *fd*($10A^{13}C$) is relatively large ($\Delta\Delta\sigma_{1/2} \approx 5$ cm^{-1}), whereas that observed for *fd*($4V^{13}C$) is negligible ($\Delta\Delta\sigma_{1/2} \approx 1$ cm^{-1}). In the former isotopomer, the 10 ^{13}C-alanines are dispersed widely through the pVIII sequence, whereas in the latter, the four ^{13}C-valines are localized exclusively near the middle of the long helix.

(b) Amide II. The amide II vibration, expected near 1550−1560 cm^{-1}, involves mainly N−H in-plane bending and C−N stretching of the trans peptide group (*22*). Because of the small change in polarizability associated with amide II, a distinct Raman amide II band usually cannot be detected in proteins. The corresponding mode (amide II^{13C}) in ^{13}C-labeled proteins is also expected to be vanishingly weak in Raman spectra. However, with peptide deuteration, the

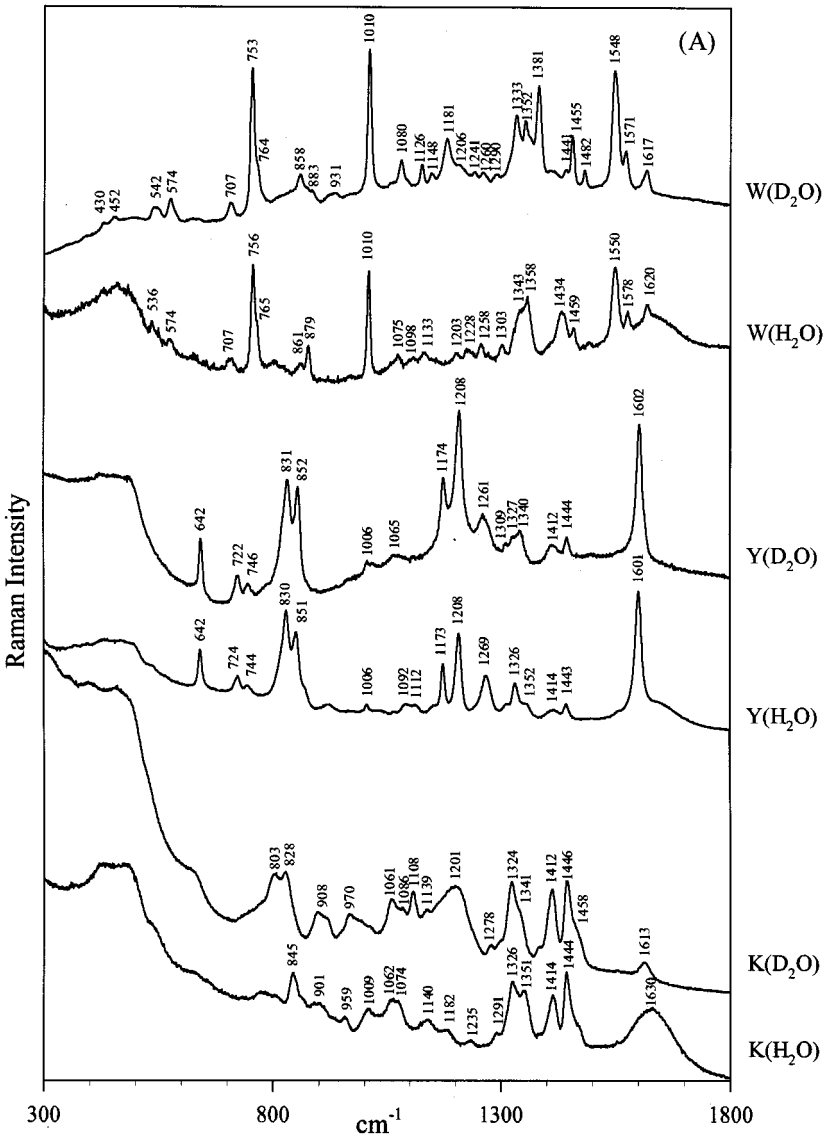

FIGURE 5: Raman spectra (300−1800 cm^{-1}) of H_2O and D_2O solutions of tryptophan (W), tyrosine (Y), and lysine (K). The pH (pD) values are near 7.0 for W and K, and near 11.0 for Y. Concentrations are in the range 50−100 mg/mL. Details are given under Materials and Methods.

nature of the normal mode is significantly altered, and the resulting amide II′ band exhibits measurable Raman intensity near 1450−1465 cm^{-1} (*41*, *42*).

The data of Figures 1−3 confirm that the amide II band of the pVIII α-helix is not detectable in Raman spectra of either *fd* or its ^{13}C-peptide isotopomers. However, as expected, the Raman amide II′ mode is observed as a major contributor to the broad band emerging at 1462 cm^{-1} upon deuterium exchange of *fd* (Figure 3).

(c) Amide III. The amide III mode involves N−H in-plane bending and C−N stretching, as well as contributions from C_α−C stretching and C═O in-plane bending. Typically, the amide III mode exhibits high Raman intensity and is highly sensitive to peptide deuteration. Sensitivity to ^{13}C labeling is also expected (*20*). Amide III in proteins can also comprise multiple band components, depending upon the types of secondary structure present and the amino acid side chains represented in the structure (*20*−*22*, *42*). In α-helical coat proteins of filamentous viruses, the Raman amide III mode(s) has (have) been assigned usually to one or more broad bands between 1270 and 1310 cm^{-1} (*3*, *5*, *35*). In contrast, amide III for the *β*-strand is expected between 1230 and 1245 cm^{-1} (*20*). It is observed near 1238 cm^{-1} in heat-denatured filamentous virus subunits (*43*). More detailed surveys of Raman amide assignments are given by Austin et al. (*42*) and Miura and Thomas (*21*).

For synthetic homopeptides, exceptions to the usual protein correlations are possible. For example, in α-helical poly(L-alanine), Raman bands observed at 1309 and 1339 cm^{-1} are shifted to 1319 and 1329 cm^{-1}, respectively, in *β*-poly(L-alanine) (*44*). Also, for poly(L-lysine), a Raman band at 1341 cm^{-1} in the α-helix form is diminished in intensity in the *β*-strand form (*45*). While these and similar results on other peptides would appear to suggest that Raman amide III markers can occur well above 1320 cm^{-1}, a more plausible explanation has been proposed recently. Spiro and co-workers (*28*, *29*) and Asher and co-workers (*27*), employing ultraviolet resonance Raman (UVRR) spectroscopy, examined the Raman band near 1380 cm^{-1} in the peptide analogue NMA. While different mechanistic interpretations have been proposed by these authors, both concur that the 1380 cm^{-1} band of NMA is associated with the C_α−H

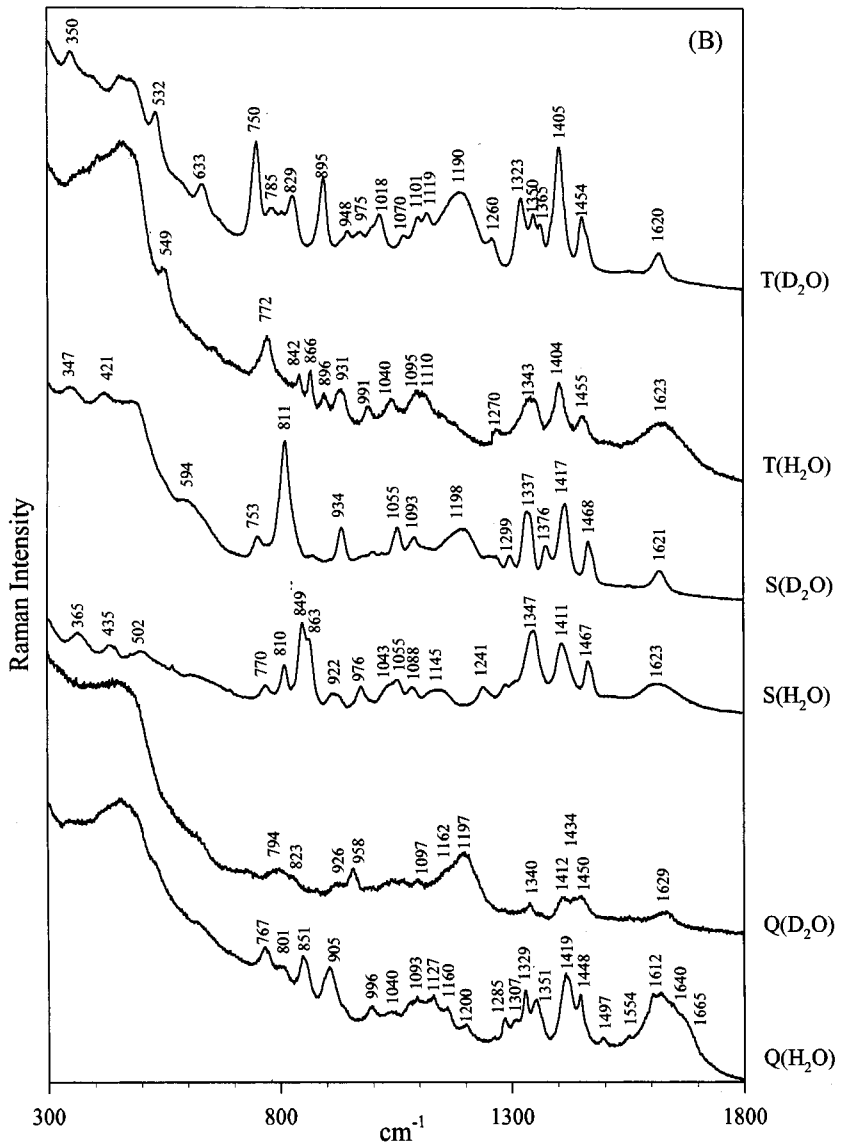

FIGURE 6: Raman spectra (300−1800 cm^{-1}) of H_2O and D_2O solutions of threonine (T), serine (S), and glutamine (Q). The pH (pD) values are near 7.0, and other conditions are as indicated in the legend of Figure 5.

bending coordinate. A similar interpretation has been given for deuteration-sensitive bands near 1340 cm^{-1} in infrared spectra of oligopeptides (*26*).

In the present off-resonance Raman study, we employ D_2O exchange of *fd* and difference spectroscopy to identify amide III (and amide III′) bands of the α-helical coat subunit. While this approach would not be adequate to assess amide intensities quantitatively, owing to uncertainties in the base line of the difference spectrum, it is sufficient to locate the principal peaks and troughs, as shown in Figure 3. Note, for example, that the points 710, 1020, and 1510 cm^{-1} serve as common tangents for both H_2O and D_2O solution spectra of the virus. Thus, we find that deuteration of *fd* diminishes intensities in the putative amide III interval for bands near 1251, 1278, and 1299 cm^{-1} (Figure 3), validating their assignment to vibrations of exchangeable groups in the virion. Further, ^{13}C labeling diminishes intensities near 1272 and 1298 cm^{-1} (Figure 1), indicating that only these two bands originate from vibrations involving the pVIII main chain. Accordingly, amide III assignments for the pVIII α-helix in native *fd* are confirmed by both deuterium and ^{13}C labeling for the bands near 1275 ± 3 and 1299 ± 1 cm^{-1}. Probable assignments for the 1251 cm^{-1} band are exchangeable side chains (glutamine, serine, and/or tryptophan) of coat subunits, or nucleoside bases (dC or dA) of packaged ssDNA. In accordance with the foregoing amide III assignments, we also assign amide III′ to the positive difference band at 949 cm^{-1} in Figure 3. This is consistent with the observed amide III′ mode of the α-helical scaffolding protein of P22 virus (*47*).

(d) The 1345 cm^{-1} Mode: A Vibration Involving both C_α−H bending and C_α−C Stretching. Interestingly, the Raman band near 1345 cm^{-1} is diminished in intensity both by ^{13}C labeling (Figure 1) and by deuteration (Figure 3) of *fd*. As seen in the difference spectra of Figures 1 and 3, the difference profiles generated near 1345 cm^{-1} are similar to those observed for the confidently assigned amide III markers near 1275 and 1300 cm^{-1}. However, the 1345 cm^{-1} band is outside the range ordinarily attributed to amide III in proteins. A more plausible assignment can be made by analogy with results obtained in the above-cited UVRR and vibrational circular dichroism studies of peptide model compounds (*26*−*28*, *41*), namely, to a vibrational mode involving both C_α−H bending and peptide group motions

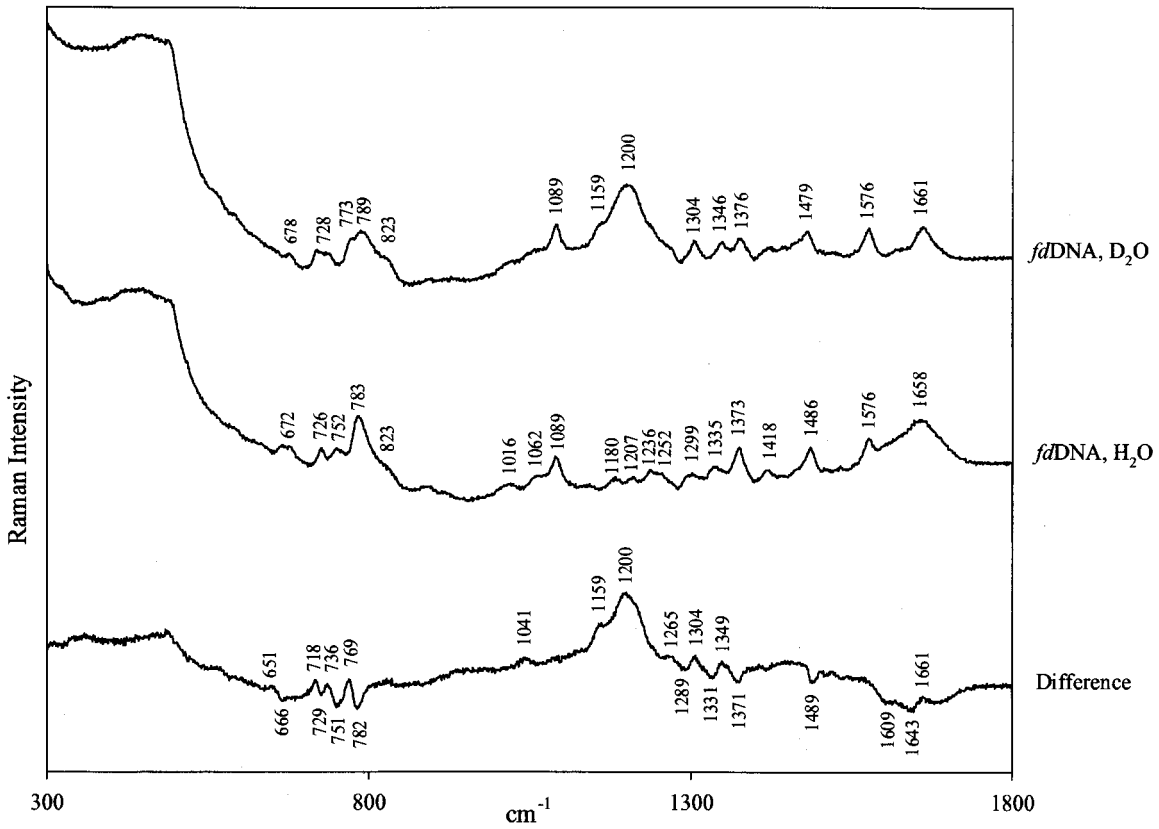

FIGURE 7: Raman spectra (300−1800 cm^{-1}) of isolated *fd* DNA in D_2O (top) and H_2O (middle) and their difference spectrum (bottom). The difference spectrum was normalized to minimize spectral differences of phosphate marker bands at 823 and 1089 cm^{-1}, which are insensitive to deuteration. The *fd* DNA concentration is approximately 30 mg/mL in solvent containing no added salt or buffering agents.

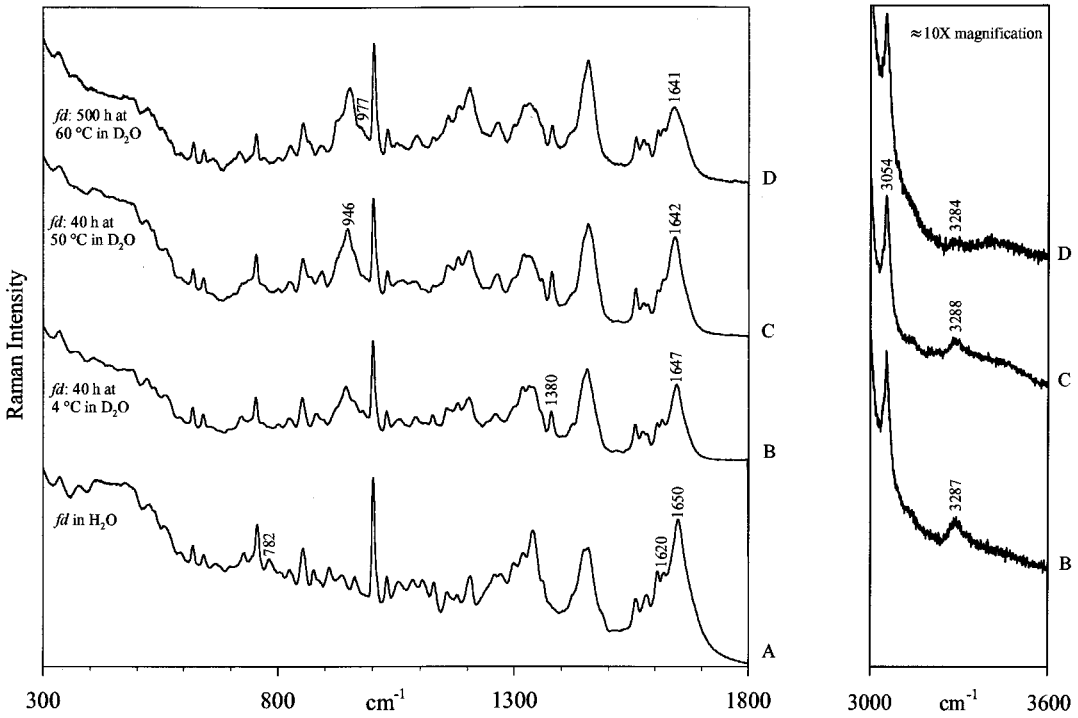

FIGURE 8: Raman spectra of *fd* in H_2O solution (trace A) and in D_2O solutions (traces B, C, and D) at different exchange conditions, as indicated at the left. The spectral intervals 300−1800 and 3000−3600 cm^{-1} are shown in the left and right panels, respectively. The integrated intensity of the band near 3287 cm^{-1} in B, C, and D is in the approximate ratio 8:4:1, respectively.

(see preceding section). To gain a better understanding of this assignment, we investigated Raman spectra of *fd* isotopomers incorporating deuterium at C_α sites of pVIII.

Figure 4 compares Raman spectra of *fd*($10A_{d1}$) and *fd* and shows that C_α deuteration of the 10 alanine sites in pVIII produces a substantial shift of Raman intensity from 1345

to 1296 cm^{-1}. The intensity loss to the 1345 cm^{-1} band is about 13%. This implies that complete C_α deuteration of pVIII would diminish the 1345 cm^{-1} band intensity by as much as 65%. The same conclusion is reached from a comparison of spectra of *fd*($10A_{d4}$) and *fd*($10A_{d3}$), which are also distinguished by the 10 $C_\alpha-D$ substituents of the former (Figure 4). Note that two types of side chains are also expected to contribute Raman intensity near 1340−1345 cm^{-1}, viz., W26 (estimated as 12% of the observed band intensity) (*14*, *30*) and the nonaromatics lysine, glycine, and serine (estimated as 19% of the band intensity) (*46*). Therefore, it is unlikely any other main-chain vibration, such as a putative amide III mode, contributes significantly near 1345 cm^{-1}. Consistent with this conclusion is the fact that no positive difference band is generated in the amide III′ interval (900−1050 cm^{-1}) accompanying C_α deuteration (data not shown). Finally, we note that the absence of a positive difference band in the 900−1200 cm^{-1} interval confirms that the 1345 cm^{-1} band is not due to a pure C−H bending vibration.

The simplest interpretation of the present results is that the $C_\alpha-H \rightarrow C_\alpha-D$ substitution accounts for most of the observed 1345 → 1296 cm^{-1} shift (frequency ratio = 1.04). Our findings indicate that this normal mode in the unlabeled pVIII helix involves $C_\alpha-H$ bending, as well as other internal coordinates. Further, the effect of ^{13}C-carbonyl labeling (Figure 1) is an indication that $C_\alpha-C$ stretching also contributes to the vibration.

(e) Amide IV. Amide IV is defined as a vibration involving C═O in-plane bending, $C_\alpha-C$ stretching, and $C-N-C_\alpha$ bending (*22*). The Raman amide IV band is expected in the 300−800 cm^{-1} interval. Based upon normal coordinate analysis of NMA (*22*), the band is probably sensitive to ^{13}C-carbonyl substitution (amide IV^{13C}) but not to peptide deuteration (amide IV′). No Raman amide IV band has yet been reported for a native protein, nor has the effect of ^{13}C labeling been tested experimentally.

Figure 1 shows that ^{13}C labeling of the *fd* coat protein diminishes Raman intensity at 741 cm^{-1}. The parent 741 cm^{-1} band, though overlapped by the intense 757 cm^{-1} band of tryptophan, is therefore assigned to amide IV of the pVIII α-helix.

(f) Other Amide Modes. A vibration involving stretching of the $N-C_\alpha-C$ skeleton is expected in the region 920−1180 cm^{-1}(*22*). Although the effect of ^{13}C-carbonyl labeling on such a stretching mode has never been demonstrated experimentally, a shift in frequency is possible. Figure 1 shows that while unlabeled *fd* generates several moderately intense Raman bands in the 920−1180 cm^{-1} region, none is significantly affected by ^{13}C labeling. Accordingly, we conclude that a main-chain vibration involving $N-C_\alpha-C$ stretching does not contribute significantly to the Raman spectrum of the pVIII α-helix. On the other hand, we note that the difference spectrum of Figure 1 gives evidence of very weak troughs centered near 1113 and 1138 cm^{-1}. These could be associated with the $N-C_\alpha-C$ linkages, but are too weak for diagnostic purposes.

Amide V (mainly C−N torsion) and amide VI (mainly out-of-plane C═O bending) modes are generally not observed in Raman spectra. Accordingly, no Raman bands in the spectrum of *fd* are assigned to these modes.

Table 1: Exchange-Sensitive Raman Bands of *fd* Virus

constituent	Raman frequency[a] *fd*	Raman frequency[a] *fd*(D_2O)	residue or group assignment[b]
pVIII main chain	1272	949	amide III; amide III′
	1298		amide III
		1462	amide II′
	1650	1637	amide I; amide I′
	3287		amide A
pVIII side chains	760	751	W26
	878	866	T, W26, Y
	908		Q15, S, T
	1055	(1041)	S, T
	1085		K, Q15, S, Y, W26
	1107		T, Y
	1130	(1123)	Q15, S, W26
	1251		S, W26
	1260		Y24
	1273	1265	Y21
	1278	(1268)	Q15, T
	1299	(1290)	K, W26
	1343	1323	K, Q15, S, T, W26
	1367	1359	W26
	1428	1380	Q15, W26
	1566	1558	W26
	1582	(1572)	W26
	1621	1617	W26
DNA[c]	675	660	dG, dT
	728	720	dA
	784	774	dC, dT
	807	800	backbone
	1492	(1482)	dG, dA

[a] Raman frequencies in cm^{-1} units are from data of Figure 3 and Figures 5−7. Values in parentheses are estimates for broad or poorly resolved bands. [b] Protein side-chain assignments are based upon data of Figures 3, 5, and 6 and results of Aubrey and Thomas (*30*), Overman (*46*), and Overman and Thomas (*14*). [c] Additional exchange-sensitive DNA bands are expected at 752, 1252, 1307, 1335, and 1373 cm^{-1} but are presumably obscured by protein contributions.

3. Other Deuteration-Sensitive Raman Bands of fd. (a) Contributions from Coat Protein Side Chains. On the basis of previous studies of simple model compounds (*48*−*50*) and the data of Figures 5 and 6, characteristic deuteration shifts are expected for Raman bands of pVIII side chains containing exchangeable NH (K, Q, W) or OH sites (S, T, Y). Most of these deuteration shifts are apparent for *fd* incubated in D_2O, as seen in the difference spectrum of Figure 3. A comprehensive assignment scheme for the exchange-sensitive bands of the pVIII side chains is proposed in Table 1. More detailed discussions are given elsewhere for exchange-sensitive Raman bands of the aromatic (W26, Y21, Y24) (*14*, *30*, *46*) and nonaromatic (K8, K40, K43, K44, K48, Q15, S13, S17, S47, S50, T19, T36, and T46) side chains of pVIII (*51*).

(b) Contributions from Packaged ssDNA. The *fd* genome constitutes only 13% of the virion mass and is expected to contribute feebly to the Raman spectrum. Nevertheless, because deuteration shifts of nucleoside Raman bands have been well characterized (*52*−*54*), the data of Figure 7 facilitate several assignments to the packaged DNA molecule. Thus, deuteration-sensitive bands of *fd* at 675, 728, 784, and 1492 cm^{-1} (Figure 3) are assigned confidently to the packaged genome, as indicated in Table 1. While many other Raman bands of packaged ssDNA are expected to shift with deuteration, including nucleoside markers at 752 cm^{-1} (dT), 1252 (dC, dA), 1307 (dA), 1335 (dA, dG) and 1373 cm^{-1} (dT, dA, dG), (Figure 7), these are obscured in the Figure 3

difference spectrum by deuteration-sensitive Raman bands of the pVIII subunit. Wen et al. (*55*) have demonstrated that these additional DNA markers can be revealed by UVRR spectroscopy of *fd* using 257 nm excitation.

Previous Raman studies of DNA fibers identify a definitive marker of the *A*-form phosphodiester conformation at 807 cm^{-1} (*56, 57*). A characteristic of the *A* marker is its insensitivity to deuteration (*57*). Therefore, while a band at 807 cm^{-1} is resolved in the spectrum of *fd*, its apparent deuteration shift to 801 cm^{-1} (Figure 3) argues against assignment to an *A*-form marker of packaged DNA. Unfortunately, the present results do not suggest another obvious assignment for the 807 cm^{-1} band of *fd*. For reasons indicated above [sections 2*(f)* and 3*(a)*], it is unlikely that the 807 cm^{-1} band originates from the main chain or side chains of pVIII. We speculate that if the band has its origin in packaged ssDNA, it is due to a backbone mode not previously encountered in protein-free DNA models. The observed deuteration sensitivity might reflect vibrational coupling with exchangeable sites, either in the covalently linked DNA bases or in protein sites coordinated with DNA phosphates. Candidates for the latter are lysine side chains.

(c) Extent of Virion Deuteration. The extent of deuteration of virion constituents (pVIII subunits and packaged ssDNA) can be estimated semiquantitatively from the present results. With respect to the pVIII main chain, resistance to deuteration following exposure to D_2O can be monitored by the persistence of an N−H stretching band near 3287 cm^{-1} (main-chain amide *A* marker), as shown in trace B of the right panel of Figure 8. (Other NH bonds of the virion, including those of DNA bases and subunit side chains, do not contribute to spectrum B of Figure 8, as noted below.) Thus, the distinct 3287 cm^{-1} band remaining in *fd* following incubation in D_2O for 40 h at 4 °C indicates that a significant number of nonexchanged NH groups persists in the pVIII main chain at these conditions. On the other hand, the population of NH groups is significantly reduced after incubation for 40 h at 50 °C (Figure 8, trace C), and is virtually eliminated after incubation for 500 h at 60 °C (Figure 8, trace D). However, the last exchange protocol, while promoting virtually complete NH → ND exchange, severely compromises the native virus assembly, as evidenced by dramatic broadening of the amide I′ marker and by the appearance of an amide III′ marker near 977 cm^{-1} (Figure 8, left panel, trace D), diagnostic of the conversion of α-helix to *β*-strand. Accordingly, we have employed the protocol of heating in D_2O for 40 h at 50 °C as the frame of reference for peptide exchange. Although exchange at these conditions is not complete, it is substantial (see below). More importantly, it is protective of the native subunit structure and *fd* assembly.

Quantitative monitoring of deuterium exchange of the pVIII main chain in native *fd* is best accomplished through use of the α-helical amide III′ marker near 950 cm^{-1}. We measured integrated areas of amide III′ bands in traces B and C of Figure 8, assuming 0% ND in trace A and 100% ND in trace D. This approach also assumes equal contributions per ND bond to the amide III′ band, irrespective of secondary structure (*58*). The results indicate approximately 86% peptide deuteration in the protocol producing spectrum C (40 h in D_2O at 50 °C) and 41% in that of spectrum B (40 h in D_2O at 4 °C). Consistent with these estimates is the accompanying 2-fold change of amide A intensity (cf. traces B and C, right panel, Figure 8).

Table 2: Raman Markers of the α-Helical pVIII Main Chain in *fd* Virus

frequency (cm^{-1})	description of mode	frequency (cm^{-1})	description of mode
1650	amide I	1345	C_α−H bending + C−C_α stretching
1637	amide I′	1298	amide III
1614	amide I^{13C}	1272	amide III
1606	amide I^{13C}	949	amide III′
1462	amide II′	741	amide IV

As noted above, the exchange-sensitive Raman band of *fd* near 784 cm^{-1} is due to cytosines of packaged DNA. Exposure of *fd* to D_2O for 40 h at 4 °C (spectrum B of Figure 8) is sufficient to completely eliminate this band in favor of the marker of the deuterated cytosine ring (ca. 771 cm^{-1}, Figure 3). No further intensity shift from 784 to 771 cm^{-1} occurs with elevation of the temperature or increase in the time of exposure to D_2O (Figure 8). A similar observation applies to the exchange-sensitive adenine marker (728 → 721 cm^{-1}), and the same may be inferred for other DNA markers of dG and dT (675 → 658 cm^{-1}). We conclude that, unlike the main chain of the pVIII subunit, the packaged DNA is completely exchanged within 40 h at 4 °C.

Similar to the bases of packaged *fd* DNA, the N1H group of the subunit tryptophan (W26) is fully exchanged within 40 h at 4 °C, as evidenced in Figure 8 by the 1380 cm^{-1} marker of the *N*-deuterated indole ring (*14, 49*).

SUMMARY AND CONCLUSIONS

Deuterium and ^{13}C have been incorporated separately into peptide groups of the α-helical coat protein subunits of the native *fd* virion. Isotopomer design, in combination with Raman spectroscopy, has provided novel vibrational assignments for the α-helix and confirmed several previously proposed assignments. In addition to Raman bands diagnostic of the isotopically unlabeled helix (amide I, amide III, and amide IV vibrations), the present work has permitted identification of Raman markers for α-helices that are deuterium-labeled at peptide nitrogen sites (amide I′, amide II′, amide III′) and ^{13}C-labeled at peptide carbonyl sites (amide I^{13C}). An unexpected finding that has resulted from investigation of the α-helix containing deuterium labeling at C_α sites is a main-chain mode at 1345 cm^{-1}. We have assigned the 1345 cm^{-1} band to a vibrational mode specific to the α-helix and involving both C−C_α−H bending and C−C_α stretching motions.

Previous Raman studies of proteins have led to the identification of other key bands in the spectral interval 1340−1360 cm^{-1}, including markers of tryptophan (Fermi doublet) (*59*) and various aliphatic side chains (*5, 46*). The tryptophan Fermi doublet is particularly important, inasmuch as the member intensities are considered diagnostic of the indole amphipathic environment (*59*). The present study shows that care must be exercised in interpreting protein Raman intensities of the 1340−1360 cm^{-1} interval, because the secondary structure of the peptide main chain may play a major role in determining the observed intensity profile.

The results summarized in Table 2 should enhance the value of Raman spectroscopy in secondary structure analyses of other protein assemblies, including filamentous viruses

of class II architecture (*Pf1* and *Pf3*). Interestingly, the coat subunit of the *Pf1* assembly lacks tryptophan, yet generates a very strong Raman band at 1345 cm^{-1}, comparable in intensity to that of *fd* (*5*) and consistent with the present conclusion that residue W26 of the *fd* coat subunit is but a minor contributor. Since the intensity of the 1345 cm^{-1} band is sensitive to salt environment in both *fd* and *Pf1* (*5*), it is reasonable to conclude that this sensitivity reflects the subunit main-chain structure rather than environments of tryptophan or other side chains. Although a definitive structural basis for the salt-dependent spectral change at 1345 cm^{-1} has not yet been established, it seems likely due either to a salt-induced change in subunit helix content or to a Raman polarization effect associated with a change in subunit (filament) orientation.

Table 2 also shows that the amide III′ marker of the α-helix is a strong and relatively sharp band centered at 949 cm^{-1}. We have used this band to estimate semiquantitatively the progress of peptide NH → ND exchange in coat subunits of the *fd* assembly. The amide III′ marker should be generally useful for assessing hydrogen exchange protection in α-helical proteins and their assemblies. Tuma et al. (*60*) have exploited this amide III′ marker to quantitatively monitor peptide exchange in the α-helical scaffolding protein of bacteriophage P22 procapsids.

Raman spectra of *fd* variants containing partial ^{13}C labeling of peptide carbonyls display unexpectedly broad amide I bands generated by the unlabeled peptide sites. We suggest that this is consistent with transition dipole coupling (amide I narrowing) in the unlabeled α-helix and decoupling (broadening) in the partially labeled helix. If correct, this interpretation would substantiate the phenomenon of TDC in a native protein structure.

The present assignment of main-chain modes and previous assignments of side-chain modes (*14*, *30*, *46*) represent together a comprehensive determination of coat protein contributions to the Raman spectrum of native *fd*. The bands remaining, which represent the contributions from the packaged ssDNA genome, are readily catalogued (Table 1). These Raman markers, like their counterparts in UVRR spectra of *fd* (*55*), are surprisingly weak in comparison to those of unpackaged DNA, indicating extraordinarily large Raman hypochromic effects for the packaged *fd* genome. The present determination of DNA Raman hypochromicity is consistent with the conclusion reached independently from UVRR results (*55*) that the bases of packaged *fd* DNA are extensively stacked.

REFERENCES

1. Webster, R. E. (1996) in *Phage Display of Peptides and Proteins* (Kay, B. K., Winter, J., and McCafferty, J., Eds.) pp 1−20, Academic Press, London.
2. Marvin, D. A., Pigram, W. J., Wiseman, R. L., Watchel, E. J., and Marvin, F. J. (1974) *J. Mol. Biol. 88*, 581−600.
3. Thomas, G. J., Jr., and Murphy, P. (1975) *Science 188*, 1205−1207.
4. Makowski, L., and Caspar, D. L. D. (1981) *J. Mol. Biol. 145*, 611−617.
5. Thomas, G. J., Jr., Prescott, B., and Day, L. A. (1983) *J. Mol. Biol. 165*, 321−356.
6. Cross, T. A., Tsang, P., and Opella, S. J. (1983) *Biochemistry 22*, 721−726.
7. Opella, S. J., Stewart, P. L., and Valentine, K. G. (1987) *Q. Rev. Biophys. 19*, 7−49.
8. Clack, B. A., and Gray, D. M. (1989) *Biopolymers 28*, 1861−1873.
9. Clack, B. A., and Gray, D. M. (1992) *Biopolymers 32*, 795−810.
10. Arnold, G. E., Day, L. A., and Dunker, A. K. (1992) *Biochemistry 31*, 7948−7956.
11. Glucksman, M. J., Bhattacharjee, S., and Makowski, L. (1992) *J. Mol. Biol. 226*, 455−470.
12. Opella, S. J., and McDonnell, P. A. (1993) in *NMR of Proteins* (Gronenborn, A. M., and Clore, G. M., Eds.) pp 159−189, CRC Press, Boca Raton, FL.
13. Marvin, D. A., Hale, R. D., Nave, C., and Helmer Citterich, M. (1994) *J. Mol. Biol. 235*, 260−286.
14. Overman, S. A., and Thomas, G. J., Jr. (1995) *Biochemistry 34*, 5440−5451.
15. Takeuchi, H., Matsuno, M., Overman, S. A., and Thomas, G. J., Jr. (1996) *J. Am. Chem. Soc. 118*, 3498−3507.
16. Overman, S. A., Tsuboi, M., and Thomas, G. J., Jr. (1996) *J. Mol. Biol. 259*, 331−336.
17. Tsuboi, M., Overman, S. A., and Thomas, G. J., Jr. (1996) *Biochemistry 35*, 10403−10410.
18. Williams, K. A., Glibowicka, M., Zuomei, L., Hong, L., Khan, A. R., Chen, Y. M. Y., Wang, J., Marvin, D. A., and Deber, C. M. (1995) *J. Mol. Biol. 252*, 6−14.
19. Miyazawa, T., Shimanouchi, T., and Mizushima, S. (1958) *J. Chem. Phys. 29*, 611−616.
20. Chen, M. C., and Lord, R. C. (1974) *J. Am. Chem. Soc. 96*, 4750−4752.
21. Miura, T., and Thomas, G. J., Jr. (1995) *Subcell. Biochem. 24*, 55−99.
22. Krimm, S., and Bandekar, J. (1986) *Adv. Protein Chem. 38*, 181−365.
23. Halverson, K. J., Sucholeiki, I., Ashburn, T. T., and Lansbury, P. T., Jr. (1991) *J. Am. Chem. Soc. 113*, 6701−6703.
24. Frushour, B. G., Painter, P. C., and Koenig, J. L. (1976) *J. Macromol. Sci.-Rev. Macromol. Chem. C15*, 29−115.
25. Mayne, L. C., Ziegler, L. D., and Hudson, B. (1985) *J. Phys. Chem. 89*, 3395−3398.
26. Diem, M., Lee, O., and Roberts, G. M. (1992) *J. Phys. Chem. 96*, 548−554.
27. Chen, X. G., Asher, S. A., Schweitzer-Stenner, R., Mirkin, N. G., and Krimm, S. (1995) *J. Am. Chem. Soc. 117*, 2884−2895.
28. Jordan, T., and Spiro, T. G. (1994) *J. Raman Spectrosc. 25*, 537−543.
29. Berkowitz, S. A., and Day, L. A. (1976) *J. Mol. Biol. 102*, 531−547.
30. Aubrey, K. L., and Thomas, G. J., Jr. (1991) *Biophys. J. 60*, 1337−1349.
31. Shin, S., and Day, L. A. (1995) *Anal. Biochem. 226*, 202−206.
32. Thomas, G. J., Jr., and Barylski, J. R. (1970) *Appl. Spectrosc. 24*, 463−464.
33. Li, Y., Thomas, G. J., Jr., Fuller, M., and King, J. (1981) *Prog. Clin. Biol. Res. 64*, 271−283.
34. Overman, S. A., and Thomas, G. J., Jr. (1998) *J. Raman Spectrosc. 29*, 23−29.
35. Williams, R. W., Dunker, A. K., and Peticolas, W. L. (1984) *Biochim. Biophys. Acta 791*, 131−144.
36. Krimm, S., and Abe, Y. (1972) *Proc. Natl. Acad. Sci. U.S.A. 69*, 2788−2792.
37. Nevskaya, N. A., and Chirgadze, Y. N. (1976) *Biopolymers 15*, 637−648.
38. Torii, H., and Tasumi, M. (1992) *J. Chem Phys. 96*, 3379−3387.
39. Reisdorf, W. C., Jr. (1994) *Protein Normal Modes: Calculations of Amide Band Positions and Infrared Intensities for Helical Polypeptides and Proteins*, Ph.D. Thesis, University of Michigan, Ann Arbor.
40. Thomas, G. J., Jr., and Agard, D. A. (1984) *Biophys. J. 46*, 763−768.
41. Wang, Y., Purrello, R., Jordan, T., and Spiro, T. G. (1991) *J. Am. Chem. Soc. 113*, 6359−6368.

42. Austin, J. C., Jordan, T., and Spiro, T. G. (1993) in *Biomolecular Spectroscopy, Part A* (Clark, R. J. H., and Hester, R. E., Eds.) pp 55−127, Wiley, London.
43. Thomas, G. J., Jr., and Day, L. A. (1981) *Proc. Natl. Acad. Sci. U.S.A. 78*, 2962−2966.
44. Fanconi, B. (1973) *Biopolymers 12*, 2759−2776.
45. Yu, T.-J., Lippert, J. L., and Peticolas, W. L. (1973) *Biopolymers 12*, 2161−2176.
46. Overman, S. A. (1996) *Raman and polarized Raman spectroscopy of the filamentous virus Ff: Structural conclusions and a molecular model*, Ph.D. Thesis, University of Missouri, Kansas City.
47. Thomas, G. J., Jr., Li, Y., Fuller, M. T., and King, J. (1982) *Biochemistry 21*, 3866−3878.
48. Lord, R. C., and Yu, N. (1970) *J. Mol. Biol. 50*, 509−524.
49. Takeuchi, H., and Harada, I. (1986) *Spectrochim. Acta 42A*, 1069−1078.
50. Takeuchi, H., Watanabe, N., and Harada, I. (1988) *Spectrochim. Acta 44A*, 749−761.
51. Overman, S. A., and Thomas, G. J., Jr. (1998) *Biospectroscopy* (to be submitted).
52. Lord, R. C., and Thomas, G. J., Jr. (1967) *Spectrochim. Acta 23A*, 2551−2591.
53. Erfurth, S. C., and Peticolas, W. L. (1975) *Biopolymers 14*, 247−264.
54. Reilly, K. E., and Thomas, G. J., Jr. (1994) *J. Mol. Biol. 241*, 68−82.
55. Wen, Z. Q., Overman, S. A., and Thomas, G. J., Jr. (1997) *Biochemistry 36*, 7810−7820.
56. Lord, R. C. (1977) *Appl. Spectrosc. 31*, 187−194.
57. Erfurth, S. C., Kiser, E. J., and Peticolas, W. L. (1972) *Proc. Natl. Acad. Sci. U.S.A. 69*, 938−941.
58. Prescott, B., Steinmetz, W., and Thomas, G. J., Jr. (1984) *Biopolymers 23*, 235−256.
59. Harada, I., Miura, T., and Takeuchi, H. (1986) *Spectrochim. Acta 42A*, 307−312.
60. Tuma, R., Parker, M. H., Weigele, P., Sampson, L., Sun, Y., Krishna, N. R., Casjens, S., Thomas, G. J., Jr., and Prevelige, P. E., Jr. (1998) *J. Mol. Biol.* (submitted for publication).

BI972339C